A contribution for the understanding of load-transfer mechanisms in multi-leaf masonry walls: Testing and modelling

Binda, L.[(1)], Pina-Henriques, J.[(2)], Anzani, A.[(1)], Fontana, A.[(1)], Lourenço, P.B.[(2)] *

[(1)] *Dept. of Structural Engineering, Politecnico di Milano, P.za Leonardo da Vinci, 32, 20133 Milano, Italy*

[(2)] *Dept. of Civil Engineering, University of Minho, Azurém, 4800-058 Guimarães, Portugal*

* Corresponding author: Tel: +351 253 510 200, Fax: + 351 253 510 217, E-mail: pbl@civil.uminho.pt

Abstract

Predicting the behaviour of multiple-leaf masonry walls is a challenging issue, given the influence of a wide range of factors as the mechanical properties of the leaves, the leaves dimensions and the way the leaves are connected to each other. In the present paper, novel experimental results in large three-leaf wallets subjected to shear and compression are introduced together with a careful numerical interpretation. Two types of collar joints (with and without shear keys) and two types of stone (weak limestone and strong sandstone) are considered in the tests. The influence of the boundary conditions on the numerical response is thoroughly investigated and good agreement with the experimental results is found. Moreover, a discussion on simplified calculations for practical assessment of existing walls is addressed.

Keywords: masonry, three-leaf walls, shear tests, compression tests, numerical modelling.

1 INTRODUCTION

Multiple-leaf masonry walls are a typology often found in historical city centres worldwide and usually consist of two or three leaves made up of different materials such as stone, brick or rubble masonry, see e.g. [1]. In the case of three-leaf walls, two outer shells and a thick inner core of rubble material are generally present. The last decades have witnessed the severe damage, or even collapse, exhibited by several famous monumental buildings due to high compressive loading in multiple-leaf pillars and walls. Recent examples are the collapse of the Cathedral of Noto, Italy, in 1996 [2] and the severe damage found in the churches of the Santissimo Crocefisso and Santissima Annunziata [3], also in Italy.

Most structural problems exhibited by three-leaf walls and pillars result from the poor or absent connection between the leaves, the weakness of the inner core or the deterioration of the mortar in the external joints. Several techniques such as grout injection or bed-joint reinforcement are today available for structural retrofitting [4,5,6]. Nevertheless, reliable safety assessment and retrofitting with minimum intervention requires proper insight on the structural behaviour and failure mechanisms, which is an especially complex issue in the case of three-leaf walls. In fact, the stress distribution is largely dependent on the mechanical properties of the leaves, on the leaves dimensions and on the way the leaves are connected to each other.

References in literature are rather scarce on this topic. Binda *et al.* [7] proposed some simple analytical models regarding two extreme situations: presence of stiff horizontal elements capable of distributing the load to the leaves proportionally to their axial stiffness and absence of such elements, making the load transfer dependent on the bond properties of the collar joints. Later on, a first experimental assessment of the

shear behaviour of two-leaf walls was reported by Binda *et al.* [8] using small scale specimens.

Egermann and Neuwald-Burg [9] carried out an extensive compression testing programme on three-leaf wallets. The experimental results showed that the outer-leaves exhibit a lower strength inside the composite system than when individually loaded and that the inner-leaves have the opposite behaviour. The different responses were attributed to the fact that the outer shells are not only compressed but are also under bending moments, and that the infill is confined.

Recently, Drei and Fontana [10] carried out a numerical study to assess the influence of different material properties and geometries in the response of multiple-leaf walls subjected to transversal loads. The results obtained indicate that large shear stress concentrations are likely to occur in keyed collar joints, which have a decisive effect on the global safety of the structure. Such stress concentrations are dependent on the leaves relative thicknesses and on the geometry of the shear keys.

The present paper illustrates an integrated experimental-numerical approach to provide understanding into the behaviour and failure mechanisms of three-leaf stone masonry walls. Experimental data on interface - shear and compression tests on large scale specimens is provided, which can contribute to the derivation of rational design rules and validation of numerical models. Firstly, the testing programme and obtained experimental data are addressed and, afterwards, the experimental results are analysed making use of simplified calculations and, also, of sophisticated numerical tools.

2 EXPERIMENTAL WORK

A set of twelve three-leaf stone wallets with dimensions of 310 × 510 × 790 mm^3, composed by two outer-leaves of ashlar masonry with mortar joints 10 *mm* thick and an inner core of rubble masonry were built and tested at the Politecnico di Milano, Italy, see Figure 1. Two types of collar joints (with and without shear keys) and two types of stones (a limestone named *Noto*, frequently used locally, and a sandstone named *Serena*, frequently used in central and southern Italy) have been considered, see Table 1. Here, it is noted that width/length ratio and height/width ratio of the tested walls have an influence on the confinement of the inner-leaf and in the compressive instability of the leaves at failure. In real-case walls transverse connections occur often between the inner and outer leaves, using ashlars or good quality masonry. A thorough study about interconnection of leaves and typical wall dimensions is needed but very difficult to carry out. In any case, extrapolation to real case walls must be very careful. The same type of stone was used for both outer and inner-leaves. The loaded faces of the wallets were caped with a cement based mortar approximately 15 *mm* thick. To minimize restraining frictional stresses Teflon sheets were placed between the wallets and the testing plates.

The tests on the wallets were carried out in a uniaxial testing machine MTS® 311.01.00, with non-rotating steel plates and a maximum capacity of 2500 *kN*. The applied load was measured by a load cell located between the upper plate and the testing machine, while displacements were recorded by a set of vertical and horizontal displacement transducers fixed to the specimens faces. In addition, the average vertical displacement of the wallets was also recorded with the testing machine in-built displacement transducer.

The wallets were tested according to three different procedures:

a) Shear tests. A monotonic load was applied to the inner-leaf while the outer-leaves were supported (triplet test). This test is similar to the EN 1052-3 [11].
b) Compression tests on single leaves. Outer and inner-leaves were tested individually under uniaxial compression.
c) Compression tests on full wallets. A monotonic load was applied to the complete transversal section of the wallets.

2.1 DESCRIPTION OF MASONRY COMPONENTS

2.1.1 *Units*

Physical and mechanical tests were carried out on cylindrical samples cored from the stone units used to build the wallets. The units were cored considering two different orientations: along the loading direction *L* and along the bedding direction *B*, so that the anisotropy of the material could be characterized.

The physical tests consisted on the determination of the bulk density and open porosity, according to EN 772-4 [12]. Six cylindrical specimens with a diameter of 80 *mm* and a height of 145 *mm* were considered for each type of stone. The average results obtained in terms of the bulk density $\rho_{b,s}$ and of the open porosity P_o are given in Table 2. In addition, the coefficient of variation *CV* is also given. The values found illustrate the significantly different physical properties of the two stones. The *Noto* limestone exhibits high open porosity and low weight while the *Serena* sandstone exhibits a 1.5 times larger weight and seven times less porosity.

Uniaxial compressive tests were carried out after the physical tests, on the same cylindrical samples, according to EN 772-1 [13]. Cutting of the specimens was arranged so that evenness and parallelism of the loading faces were assured and, in this way, capping could be avoided. The height of the specimens was limited by the 150 *mm* height of the stone units from which the specimens were extracted and, for this reason, a height over diameter ratio less than 2.0 was utilized. The ASTM standard C39 [14] accounts for the effect of ratios less than 2.0 in concrete specimens by introducing a correction factor. For the ratio adopted in the experiments, 1.75, the reduction factor equals 0.98, which is quite small when compared with the data variability and, thus, was not considered. Three specimens for each combination type of stone/orientation were tested.

The average values for the compressive strength f_c, peak strain ε_p, modulus of elasticity E and coefficient of Poisson ν are given in Table 3. It is noted that E and ν were calculated, in general, between 30 and 60% of f_c. According to the results obtained, the *Serena* stone exhibits, in the loading direction, a strength about five times larger than the *Noto* stone and about the double of the stiffness.

The tensile strength was obtained by the splitting test, which is an indirect tension test. This test is not yet specified by a European standard and the RILEM recommendation for concrete CPC6 [15] was adopted. The tests were carried out on six cylindrical specimens for each type of stone with a diameter and height of 80 *mm*. The specimens were obtained by sawing in half three cylinders cored along the bedding direction of the units. This direction is the most relevant with respect to the tensile strength as is the direction where the principal tensile stresses occur when units are vertically loaded.

The average results obtained are given in Table 4. In the case of concrete, the splitting tensile strength $f_{t,s}$ is about 5 to 12% higher than the direct tensile strength f_t [16]. Here, f_t has been considered equal to 0.9 $f_{t,s}$. According to the results obtained, the *Noto* stone exhibits an average tensile strength three times smaller than the *Serena* stone. Concerning the ratio between the compressive and tensile strengths, a value of ten times was found for the *Noto* stone and a value of seventeen times was found for the *Serena* stone.

2.1.2 *Mortar*

A commercial premixed hydraulic lime mortar denominated *Albaria Allettamento*, Italy, was adopted to build the wallets. Flexural and compressive tests have been carried out according to EN 1015-11 [17]. The flexural tests were carried out on $40 \times 40 \times 160$ mm^3 prisms casted in steel molds. Noteworthy, with this procedure the water absorption effect of the units is ignored and thus these specimens are not fully representative of the mortar inside the composite, see e.g. [18]. The compressive tests were carried out after the flexural tests on the two resulting halves of the prisms. The tests were performed at four ages: 28 days, 75 days (corresponding to the beginning of the tests), 90 days and 172 days (corresponding to the end of the testing programme). For each curing stage a total of six prisms were tested.

Table 5 gives the average results obtained for the flexural strength f_f and for the compressive strength f_c. The results found yield average values for the flexural and compressive strengths during the testing period (75 to 172 days) of 2.2 N/mm^2 and 10.3 N/mm^2. Generally, a factor of 1.5 can be assumed for the ratio between the flexural and tensile strengths, see Van der Pluijm [19] and Lourenço [20].

2.2 RESULTS OF SHEAR TESTS

Two wallets for each combination type of stone - type of connection were tested in a total of eight specimens. The load-displacement diagrams obtained using the in-built displacement transducer of the testing machine are illustrated in Figure 2. In the case of the wallets with straight collar joints, a non-symmetric response of the connections was found, with failure occurring non-simultaneously. Such behaviour had also been found by Lourenço *et al.* [21], Binda *et al.* [8,22] and Mirabella Roberti *et al.* [23] and must be considered characteristic of the triplet test.

The first peak in the diagrams of Figure 2a corresponds to the failure of the weakest connection and provides the shear strength τ_r for a shear area of $2 \times 310 \times 790\ mm^2$. After failure of the first connection a minor rotation of the two leaves still connected was observed due to the eccentricity of the applied load. From that point on the test cannot be intended as a triplet test due to the change in the loading scheme and, therefore, the values related to the second connection to fail should be considered carefully. Namely, the second peak represents the combination of a higher shear strength for the second joint and some minor friction in the first joint due to bending. If the effect of bending is neglected, the second peak provides the shear strength of the strongest joint τ_r', for a shear area of $310 \times 790\ mm^2$. This holds true only because no confining pressure is present.

For the wallets with keyed collar joints, the shear strength was calculated assuming straight connections and, thus, the value represents an "equivalent" shear strength. Table 6 gives, in the case of straight collar joints wallets, the average shear strengths (τ_r and τ_r') and displacements (δ and δ') corresponding to the first and second

load peaks. For keyed collar joints wallets, the average values of the shear strength and the corresponding displacements are given.

From the results obtained it is possible to observe that while the shear strength of straight collar joints wallets is mainly influenced by the physical properties of the stone, like the porosity that is closely related to the stone-mortar adhesion, in the case of keyed collar joints wallets the strength of the stone is a major issue.

In terms of ductility, the specimens with straight collar joints show a similar behaviour for both types of stones. The failure is quite brittle and without showing any residual strength, given that the test set-up allows the wallets to move freely outwards. Regarding the wallets with keyed collar joints, the *Serena* specimens exhibit a less brittle behaviour than the *Noto* specimens.

Figure 3 illustrates relative shear displacements at the connections recorded by "short" transducers (*T3*, *T5*, *T10* and *T11*) and "long" transducers (*T4* and *T12*), employed as shown in Figure 4.

Failure of the connections in the *Noto* wallets occurred in a quite brittle manner as can be verified by the behaviour of the "short" transducers, which show zero values until near the peak load, see *T10* and *T11* in Figure 3a. However, it can still be observed that the connection does not fail all at once but that the crack rapidly develops from the top (*T11*) to the bottom (*T10*). The "long" transducers behave in a quite different manner, showing increasing shortening until initiation of the shear cracks, with subsequent inversion of the trend and sudden elongation, see *T4* in Figure 3a. Such behaviour can be explained by the fact that "long" transducers are not only measuring shear slippage at the connection but are also influenced by the deformation of the leaves.

On the contrary, *Serena* wallets with straight collar joints show a progressive development of the shear cracks since an early stage, yielding a less brittle failure than the *Noto* wallets. This behaviour is confirmed by the diagrams of the "short" transducers *T3* and *T5* shown in Figure 3b. This different behaviour can be explained by the weak adhesion between the *Serena* stone and the mortar.

Regarding the wallets with keyed collar joints it can be observed from Figure 5 that the transducers positioned in the outer-leaves above the central indentation (*T10* and *T12* in Figure 6) exhibit, initially, an increasing shortening as expected. However, after a determined load level the transducers start to show an elongation. Such behaviour can be attributed to the fact that the two upper courses of the wallets are being pushed outwards by the applied load. It can also be observed that the transducers positioned in the inner-leaf above the central indentation (*T11*) show larger deformations than the correspondent transducers below them (*T14*). This can be observed in a rather clear manner up to a certain load level, before transducers become disturbed by the appearance of cracks. Such behaviour results from the load transfer between inner and outer-leaves. This process cannot be observed so clearly in the outer-leaves, partly due to the complex behaviour of transducers *T10* and *T12*, as explained above.

Typical ultimate crack patterns are illustrated in Figure 7. The wallets with straight collar joints failed due to the development of two vertical shear cracks along the connections. No other visible damage was observed at the end of the test.

In the case of the specimens with keyed collar joints, the cracking pattern was different according to the type of stone. For the *Noto* specimens, damage was observed in both outer and inner-leaves. In the inner-leaves, more severely damaged, diagonal cracks were observed, developing from the shear keys and passing through the inner-

leaf stones. Concerning the outer-leaves, diagonal cracks near the base appeared. At ultimate stage, full separation in three irregular leaves could be observed.

In the *Serena* specimens, the cracks developed only in the inner-leaf. However, in this case, cracks usually went around the stones instead of breaking them, due to the larger strength and smaller stone-mortar adhesion. At ultimate stage, it is clearer to observe that only the inner-leaf collapsed.

2.3 RESULTS OF COMPRESSION TESTS ON SINGLE LEAVES

The tests were performed on the leaves of the wallets with straight collar joints, previously tested in shear, see Section 2.2. In the case of the *Noto* specimens, both outer-leaves were tested simultaneously, trying to reproduce what may happen in real composite walls: shear failure of the connections followed by transfer of almost all the load to the external stiffer elements. This can explain the type of damage found in massive pillars, see Binda *et al.* [2]. In the case of the *Serena* leaves, which were much more resistant, the same procedure could not be adopted due to the limited capacity of the testing machine and, thus, the leaves had to be tested separately.

A comparison between the stress-strain diagrams obtained for the outer and inner-leaves using the in-built displacement transducer of the testing machine is shown in Figure 8. The average results obtained, including the strength f_c, the peak strain ε_p, the elastic modulus E and the Poisson coefficient ν are given in Table 7.

From the given results it is observed that the *Noto* outer-leaves exhibit a strength of about 45% the stone strength and the inner-leaf about 20%. In the case of the *Serena* leaves, the same ratios are about 40% for the outer-leaves and only 4% for the inner-leaf, which stresses the major influence of the mortar in the inner-leaf failure. It is

further noted that the *Serena* inner-leaves exhibit a less brittle behaviour than the *Noto* specimens, again due to the higher strength of the stones, forcing cracks to go around them instead of passing through.

Figure 9 to Figure 12 illustrate selected stress-strain diagrams obtained from the displacement transducers fixed to the specimens as well as their position. As can be observed, the diagrams of the outer-leaves are much more disturbed by the development of cracks than the diagrams of the inner-leaves and a conclusion can be hardly withdrawn from the collected data. Concerning the inner-leaves, it can be observed that the leaves built with the *Serena* stone show a less brittle behaviour than the *Noto* leaves. Typical failure patterns are illustrated in Figures 13 and 14 for the outer and for the inner-leaves, respectively. The shaded areas indicate spalling of the stone.

2.4 RESULTS OF COMPRESSION TESTS ON FULL WALLETS

One wallet of each type (stone/connection combination) was tested in compression, in a total of four specimens. Yet, the peak load for the *Serena* wallets was beyond the capacity of the testing machine and a maximum load of 2380 *kN* was applied. The stress-strain diagrams obtained using the in-built displacement transducer of the testing machine are shown in Figure 15. Table 8 gives the results found.

The following observations can be made from the results, even if the limited number of tests precludes any conclusive statement:

a) The strength of the *Noto* wallet with keyed collar joints seems to be about 10% higher than the wallet with straight collar joints.
b) The *Noto* wallet with keyed collar joints seems to exhibit a less brittle behaviour than the wallet with straight collar joints.

c) The peak load of any of the two *Noto* wallets tested is not much higher than the peak load of the single outer-leaves (912.3 *kN*), although the cross-sectional areas are different and, hence, the strength.

The stress-strain diagrams obtained with the transducers fixed to the specimens as well as the transducers position are shown in Figures 16 and 17 for wallets with straight collar joints, and in Figures 18 and 19 for wallets with keyed collar joints. Larger vertical strains were found in the outer-leaves than in the inner-leaves for wallets with straight collar joints, see Figure 16. Such behaviour is not completely clear but can be attributed to bedding of the inner-leaf prior to testing, which prevented mobilization of the inner-leaf bearing capacity. On the contrary, in the case of wallets with keyed collar joints, vertical strains in the different leaves are rather similar, emphasising the role of shear keys in obtaining a uniform distribution of strains, see Figure 18.

Such behaviour can also be confirmed by comparing the horizontal deformation of the wallets (given by *T8* and *T15*) with the horizontal strain of the inner-leaves (*T5* and *T12* for straight collar joints wallets and *T9* and *T14* for keyed collar joints wallets), which shows that only in the case of keyed wallets the inner-leaf is deforming since the beginning of the test. Finally, it should be referred that transducers *T8* and *T15* on Figure 16b exhibit an unexpected behaviour. This is probably due to a minor inclination of the outer-leaves prior to testing.

The failure patterns observed are illustrated in Figures 20 and 21. The shaded areas indicate spalling of the stone. The *Noto* wallet with straight connections failed due to the development of several vertical cracks in the outer-leaves while the inner-leaf was practically undamaged.

In the case of the *Noto* wallet with keyed connections, the outer-leaves exhibited a more severe and diffuse cracking pattern with several vertical cracks developing in the

inner-leaf near the peak load. Regarding the *Serena* wallet with keyed connections and despite the fact that the peak load was not attained, the development of some cracks in the inner-leaf could be observed.

3 SIMPLIFIED CALCULATIONS

This section contains a first analytical interpretation of the experimental results, with simple calculations being used to predict the compressive strength of the wallets. It is noted that the experimental results found should be considered as indicative and conclusions should be taken carefully due to the small number of specimens.

The compressive strength of composite sections f_c can be estimated making use of the following equations, each one assuming different hypotheses:

a) the external load is completely supported by the stiffer elements, i.e., the outer-leaves:

$$f_c = \frac{2\,t_e}{2\,t_e + t_i} \cdot f_e \tag{1}$$

b) the external load is supported by each leaf according to its cross-sectional area ratio:

$$f_c = \frac{2\,t_e}{2\,t_e + t_i} \cdot f_e + \frac{t_i}{2\,t_e + t_i} \cdot f_i \tag{2}$$

c) the external load is supported by each leaf according to its area ratio and adjusted by a correction factor, see Egermann and Neuwald-Burg [9]:

$$f_c = \frac{2\,t_e}{2\,t_e + t_i} \cdot \theta_e \cdot f_e + \frac{t_i}{2\,t_e + t_i} \cdot \theta_i \cdot f_i \tag{3}$$

In the above, t_e and t_i are the thicknesses of the outer and inner-leaves and f_e and f_i are the uniaxial compressive strengths of the outer and inner-leaves. The parameters θ_e and θ_i are correction factors for the outer and inner-leaves, assuming that the outer-leaves are under biaxial compressive stresses and bending moments and, thus, their uniaxial strength should be reduced and that the inner-leaf is under a multi-axial compressive state of stress and, therefore, its uniaxial strength should be increased.

The results obtained for the wallets with and without shear keys are given in Table 9. In the case of the wallets with keyed collar joints, the thickness assumed for the inner-leaf includes the length of the shear keys. With respect to the application of Eq. (3), the values adopted for the correction parameters were $\theta_e = 0.7$ and $\theta_i = 1.3$, see [9]. It is further noted that Eq. (1) was not used to estimate the strength of the wallets with keyed joints because, in this case, it is clear that the inner-leaf is collaborating in the composite response.

The value predicted for the compressive strength of the wallets with straight collar joints using Eq. (1) and Eq. (3) show an excellent agreement with the experimental results, see Table 9. Note that, however, the fact that the experimental and the predicted values are exactly the same should be considered as just a coincidence. The stress-strain diagrams illustrated in Figure 22a show that the inner-leaf vertical deformations do not accompany the vertical deformations of the outer-leaves and that, at failure, the inner-leaf strain is quite less than its peak strain when individually tested, see also Figure 23a. As a consequence, the bearing capacity of the inner-leaf is only partially mobilized and the hypothesis of Eq. (1) holds fairly true. Again, the causes for the different deformations in the wallet leaves are not completely clear but a possible reason may be attributed to settling of the inner-leaf prior to testing.

In the case of the wallets with keyed collar joints, Eq. (2) yielded the best result while the strength predicted by Eq. (3) is less than the experimental value for the *Noto* wallets. This indicates that the inner-leaf is collaborating in the wallets response, as confirmed by Figures 22b and 23b, but the assumptions of a strength reduction of the outer-leaves due to bending and a strength increase of the inner-leaf due to confinement do not apply. This can be explained by the test boundary conditions, which allow horizontal displacements to occur at the top and bottom of the wallets. In such way, the effects of outer-leaves bending and inner-leaf confinement are diminished.

Finally, it should be noted that each equation considered independently predicts a larger strength for the wallets with straight collar joints than for the wallets with keyed collar joints. This is due to the reduction of the cross-sectional area of the outer-leaves in the case of the specimens with shear keys. However, the opposite behaviour was found in experiments. The reason of such behaviour can be attributed to the fact, as already mentioned, that the inner-leaf was almost not collaborating in the experimental response in the case of wallets with straight collar joints.

4 NUMERICAL SIMULATIONS

This section deals with the numerical simulation of the experimental tests, contributing to the results interpretation. The leaves of the wallets were represented using plane stress continuum elements (8-noded) with 2 × 2 Gauss integration while line interface elements (6-noded) with 3 × 3 Lobatto integration have been adopted for the collar joints. The analyses were carried out with indirect displacement control with line searches. It is further noted that the self-weight of the wallets was not considered.

For the material behaviour, a composite plasticity model with a Drucker-Prager yield criterion in compression and a Rankine yield criterion in tension was adopted. The inelastic behaviour exhibits a parabolic hardening/softening diagram in compression and an exponential-type diagram in tension. The material behaves elastically up to one-third of the compressive strength and up to the tensile strength. For the interface elements a combined cracking-shearing-crushing model developed by Lourenço [24] was adopted. The compressive mode was, however, not active and interface failure could only occur by shear or/and tensile yielding. Both shear and tensile modes exhibit exponential-type softening.

The elastic material properties adopted for the wallets leaves are given in Table 10 and the inelastic properties in Table 11. Here, E is the elastic modulus, ν is the Poisson coefficient, c is the cohesion, f_t is the tensile strength, ϕ is the friction angle, ψ is the dilatancy angle, Gf_c is the (cohesion related) compressive fracture energy and Gf_I is the tensile fracture energy.

The cohesion was obtained from Eq. (4), which derives from the Drucker-Prager yield function applied to uniaxial compression. Here, f_c is the compressive strength. The tensile strength of the outer-leaves was considered equal to the tensile strength of the stone, assuming, thus, vertical cracking. The tensile strength of the inner-leaf was obtained according to $f_t = f_c / 1.5$, which is a relation often found for masonry specimens. The value adopted for the friction angle ϕ was 10º (a larger value in plane-stress would implicate an overestimation of the biaxial strength for this specific yield criterion) and, for the dilatancy angle ψ, a value of 5º was assumed. Please note that the adopted values cannot be directly compared with the values of the angles usually adopted for the Mohr-Coulomb criterion. For the tensile fracture energy, a value in agreement with the experimental results reported by Van der Pluijm [19] for brick

specimens was adopted. The values of the elastic modulus and of the compressive fracture energy were adopted so that the numerical response of the specimens best fitted the experimental response, see Figure 24.

$$c = \frac{1 - \sin\phi}{2\cos\phi} f_c \tag{4}$$

The elastic material properties assumed for the collar joints are given in Table 12 and the inelastic properties are given in Table 13. The parameters were obtained, whenever possible, from the shear test on wallet *NS1* but most of the inelastic parameters were unknown and had to be estimated. The interfaces shear stiffness k_s was adopted so that the numerical and experimental elastic responses showed a good agreement. Based on elastic assumptions, the normal stiffness k_n can be obtained according to $k_n = k_s \times 2\ (1 + \nu) = 1.0\ N/mm^3$, where $\nu = 0.2$ is the coefficient of Poisson. However, higher values had to be adopted in order to avoid interpenetration of the two continuums separated by the interfaces.

The cohesion c for the first connection to fail was given experimentally but for the second connection a value was adopted so that the numerical response resembled the experimental response. The values of the remaining inelastic parameters (tensile strength f_t, friction coefficient $tan\phi$, dilatancy coefficient $tan\psi$, mode I fracture energy Gf_I and mode II fracture energy Gf_{II}) were adopted in agreement with the values experimentally found by Van der Pluijm [19] and recommended by Lourenço [25] for unit-mortar interfaces.

4.1 SHEAR SIMULATIONS

The shear tests for both types of wallets, either with or without shear keys, have been numerically reproduced. As it will become clear later in the text, the testing boundary conditions are a key issue for the correct interpretation of the results. The experimental test set-up was composed by two steel plates at the bottom, supporting the outer-leaves, and a third plate over the inner-leaf, through which a vertical load was applied. Additionally, sheets of Teflon were placed between the steel plates and the wallets. Therefore, the shear interaction between the plates and the wallets is not a clear issue and must be further investigated.

For the wallets with straight collar joints, this aspect has been assessed by considering four different shear stiffnesses k_s at the supports:

a) $k_s = 0$, the specimen is free to slide over the steel plates.

b) $k_s = \infty$, shear slip is precluded between the specimen and the plates.

c) Constant $k_s = 0.01\ N/mm^3$, an intermediate constant shear stiffness is applied and, thus, shear slip can occur but the horizontal reactions at the boundaries increase with increasing displacement.

d) Non-linear k_s. At the level of the upper plate, shear slip is free to occur up to a certain relative displacement, beyond which, shear slip is completely restrained. A transition phase for k_s was also considered. At the level of the bottom supports, shear slip is precluded.

Regarding the normal stiffness k_n given to the boundaries, the same behaviour was adopted for all cases. Zero stiffness in tension and infinite stiffness in compression were considered. Figure 25 illustrates the experimental load-displacement diagram obtained for the wallet *NS1* and the numerical diagrams obtained according to the

different boundary conditions. It is noted that the two experimental load peaks correspond to the failure of each connection.

Regarding the numerical diagrams, for boundaries with $k_s = 0$, after failure of the first connection the specimen starts sliding until complete degradation of strength and, thus, only one of the two connections fails. Another interesting point is that the collapse load is underestimated. Such difference is due to the absence of horizontal constraints at the bottom, which leads to a failure that is not exclusively governed by shear but is accompanied also by flexural tensile stresses.

For supports with $k_s = \infty$, a smooth load drop due to material softening follows the failure of the first connection. Yet, it is not as sudden or as deep as the experimental load drop. In terms of collapse loads, the first load peak shows a good agreement with the experimental results but the second load peak, corresponding to the failure of the second connection, is largely overestimated. This is, again, due to the softening behaviour of the first connection to fail, which is still contributing to the specimen strength when the second connection fails.

For a constant shear stiffness $k_s = 0.01\ N/mm^3$, the value of the first load peak equals the value for $k_s = 0$ and, thus, is also underestimated. After the failure of the first connection, the specimen starts sliding over the boundaries with the load suddenly dropping. However, in this case, after some amount of shear slip, the horizontal reactions at the supports become mobilized and a load increase is observed until failure of the second connection occurs. The comparison with the experimental response shows, nevertheless, that an understiff response was obtained for the second increasing branch.

These results demonstrate that to capture correctly the experimental behaviour, the boundary conditions adopted must allow some amount of shear slip at the supports

after the failure of the first connection and, afterwards, restrain it completely. Therefore, a non-linear k_s was adopted for the upper boundary together with complete shear slip restriction at the bottom boundaries. Good agreement with the experimental response was found, see Figure 25b. Even so, the slope of the second increasing branch is slightly underestimated. This shows that the hypothesis assumed of equal shear stiffness for the two connections is, probably, not true for this specimen, with the second connection showing a stiffer behaviour than the first connection. Figure 26 depicts the progressive shear failure of the wallet.

In the case of keyed collar joints wallets, the influence of the boundary conditions in the response was assessed by a similar procedure. Here, three different shear stiffnesses at the boundaries were considered: (a) $k_s = 0$, (b) $k_s = \infty$ and (c) an intermediate constant $k_s = 2.0\ N/mm^3$.

The comparison between the numerical and the experimental load-displacement diagrams is given in Figure 27. The deformed meshes at failure for each numerical diagram are depicted in Figure 28. The collapse load obtained for zero shear stiffness at the boundaries is significantly lower than the experimental collapse load. In this situation, the specimen fails due to a vertical crack that arises in the weaker connection (left), developing along the shear keys. For infinite shear stiffness at the boundaries, a much better agreement with the experimental collapse load is found. Here, failure is governed by crushing of the inner-leaf near the top.

In the experimental failure mechanism, both described modes seem to be present and, thus, an intermediate k_s was considered in order to reproduce more accurately the behaviour found. The collapse load obtained was almost the same as for $k_s = \infty$ and is about 80% of the experimental collapse load. In this case, failure occurs due to

combined shearing-crushing of the inner-leaf near the top and due to the development of vertical cracks along the shear keys, see Figure 28c.

For the intermediate k_s at the supports, Figure 29 illustrates the contour of minimum principal stresses for the elastic regime and the principal plastic strains at failure. In Figure 29a, it is visible the transfer of compressive stresses from the inner-leaf to the outer-leaves, through the shear keys. In Figure 29b,c, the shearing-crushing of the inner-leaf near the top and the tensile damage in the inner-leaf, along the shear keys, is confirmed as failure mechanism.

4.2 COMPRESSION SIMULATIONS ON FULL WALLETS

The compression tests on wallets with and without shear keys have also been analysed. Friction between wallets and boundaries has been precluded in the simulations. In the case of the wallet with straight connections, a row of mesh elements at middle height was made slightly imperfect and a 10% lower compressive strength was given. The objective is to trigger the strain localization.

A comparison between numerical and experimental stress-strain diagrams is given in Figure 30. Good agreement is found in the case of the wallet with keyed collar joints. In the case of the wallet with straight collar joints, the predicted strength is about 20% higher than the experimental strength. As discussed in Section 3, the inner-leaf is almost not collaborating in the experimental response, which can partially explain the difference found between the experimental and numerical strength values.

Another point is that the numerical strength of the wallet with keyed connections is lower than the strength of the wallet with straight connections, as predicted also by the simple expressions discussed in Section 3. Such behaviour is explained by the smaller cross-sectional area of the outer-leaves in the case of the

wallets with keyed collar joints, for which a reduced thickness of 130 *mm* was adopted for the courses without shear keys. On the contrary, the outer-leaves of wallets with straight collar joints have a constant thickness of 170 *mm*. Concerning the failure patterns, it is stressed that, of course, continuum finite element models can not realistically reproduce the propagation of cracks typical of compressive failure. The numerical failure patterns obtained are just phenomenological and consist of localization of deformation in a single finite element, as typical of strain softening or non-associated plasticity models.

5 CONCLUSIONS

The present paper addresses the load-transfer in composite masonry walls, which seems to be not a sufficiently debated issue in literature. From the experimental tests, the following conclusions can be drawn:

a) Shear strength values found for straight collar joints are between 0.09 - 0.17 N/mm^2, whereas for keyed joints the values are in the 0.58 - 0.81 N/mm^2 range.

b) In wallets with straight collar joints, shear failure occurs due to vertical cracks that arise in the connections while in wallets with keyed collar joints, failure is mainly due to the development of inclined cracks in the inner-leaf.

Numerical assessment of the experimental data was also addressed by utilizing a plasticity based finite-element model, in which units and mortar were smeared out in a continuum. The influence of the boundary conditions on the response was investigated and good agreement with the experimental results has been found.

Simplified calculations for predicting the compressive strength of composite walls have also shown good agreement with experimental results and with advanced numerical methods. Thus, simplified expressions may be used as a first estimate of the

wallets strength. It is stressed that width/length ratio and height/width ratio of the tested wallets have an influence on the confinement of the inner-leaf and in the compressive instability of the leaves at failure. Thus, extrapolation to real-case walls must be very careful.

Suggestions for future work include further compression testing on composite wallets, considering also specimens with different ratios between inner and outer-leaves thicknesses.

ACKNOWLEDGEMENTS

The experimental research was supported by MURST (cofin. 2000/2002). The financial support by the Portuguese Foundation for Science and Technology under grant SFRH/BD/5002/2001 awarded to the second author is gratefully acknowledged. Authors wish to thank M. Antico for technical assistance and M. Brazzale for data elaboration.

REFERENCES

[1] Binda L, Palma M, Penazzi D. Cautious repair of stone-masonry structures in seismic areas. In: Proc Int Conf of the SFB315 Research Centre of Karlsruhe University. Karlsruhe, Germany; 1999. p. 99-108.

[2] Binda L, Saisi A, Benedictis R De, Tringali S. Experimental study on the damaged pillars of the Noto Cathedral. In: Proc 8th Int Conf on Structural Studies, Repairs and Maintenance of Heritage Architecture. Halkidiki, Greece; 2003. p. 89-98.

[3] Binda L, Saisi A, Messina S, Tringali S. Mechanical damage due to long term behaviour of multiple-leaf pillars in Sicilian churches. In: Proc 3rd Int Sem on Historical Constructions. Guimarães, Portugal; 2001. p. 707-18.

[4] Vintzileou E, Tassios TP. Three-leaf stone masonry strengthened by injecting cement grouts. Journal of Structural Engineering, ASCE, 1995;121(5):848-56.

[5] Valluzzi MR, Porto F Da, Modena C. Behaviour and modelling of strengthened three-leaf stone masonry walls. Materials and Structures, RILEM, 2004;37(267):184-92.

[6] Toumbakari EE. Lime-pozzolan-cement grouts and their structural effects on composite masonry walls. PhD thesis. Leuven Catholic University, Belgium; 2002.

[7] Binda L, Fontana A, Anti L. Load transfer in multiple-leaf masonry walls. In: Proc 9th Int Brick/Block Masonry Conf. Berlin, Germany; 1991. p. 1488-97.

[8] Binda L, Fontana A, Mirabella Roberti G. Mechanical behaviour and stress distribution in multiple-leaf walls. In: Proc 10th Int Brick/Block Masonry Conf. Calgary, Canada; 1994. p. 51-9.

[9] Egermann R, Newald-Burg C. Assessment of the load bearing capacity of historic multiple-leaf masonry walls. In: Proc 10th Int Brick/Block Masonry Conf. Calgary, Canada; 1994. p. 1603-12.

[10] Drei A, Fontana A. Influence of geometrical and material properties on multiple-leaf walls behaviour. In: Proc 7th Int Conf on Structural Studies, Repairs and Maintenance of Heritage Architecture. Bologna, Italy; 2001. p. 681-91.

[11] CEN. Methods of test for masonry: Determination of initial shear strength. EN 1052-3. Brussels (Belgium): CEN; 2002.

[12] CEN. Methods of test for masonry units: Determination of real and bulk density and of total and open porosity for natural stone masonry units. EN 772-4. Brussels (Belgium): CEN; 1998.

[13] CEN. Methods of test for masonry units: Determination of compressive strength. EN 772-1. Brussels (Belgium): CEN; 2000.

[14] ASTM. Test method for compressive strength of cylindrical concrete specimens. 04.02-C39. Annual book of ASTM standards. Philadelphia (USA): ASTM; 2004.

[15] RILEM. Tension by splitting of concrete specimens. CPC6. Compendium of RILEM Technical Recommendations. London (UK): E&FN Spon; 1994.

[16] Neville A. Properties of concrete. New York (USA): Wiley; 1997.

[17] CEN. Methods of test for mortar for masonry: Determination of flexural and compressive strength of hardened mortar. EN 1015-11. Brussels (Belgium): CEN; 1999.

[18] Lourenço PB. Computational strategies for masonry structures. PhD thesis. Delft University of Technology, The Netherlands; 1996. Available from http://www.civil.uminho.pt/masonry.

[19] Pluijm R Van der. Out-of-plane bending of masonry: behaviour and strength. PhD thesis. Delft University of Technology, The Netherlands; 1999.

[20] Lourenço PB. An anisotropic macro-model for masonry plates and shells: implementation and validation. Report 03.21.1.31.07. Delft University of Technology, The Netherlands; 1997. Available from http://www.civil.uminho.pt/masonry.

[21] Lourenço PB, Barros JO, Oliveira JT. Shear testing of stack bonded masonry. Construction and Building Materials, 2004;18(2):125-32.

[22] Binda L, Fontana A, Mirabella Roberti G. Modelling of the mechanical behaviour of multiple-leaf stone walls. In: Proc Int Symp on Computer Methods in Structural Masonry. Swansea, UK; 1993. p. 229-41.

[23] Mirabella Roberti G, Binda L, Cardani G. Numerical modelling of shear bond tests on small brick-masonry. In: Proc 4th Int Symp on Computer Methods in Structural Masonry. Florence, Italy; 1998. p. 144-152.

[24] Lourenço PB, Rots JG. A multi-surface interface model for the analysis of masonry structures. J of Engineering Mechanics, ASCE, 1997;123(7):660-8.

[25] Lourenço PB. A user/programmer guide for the micro-modelling of masonry structures. Report 03.21.1.31.35. Delft University of Technology, The Netherlands; 1996. Available from http://www.civil.uminho.pt/masonry.

FIGURES

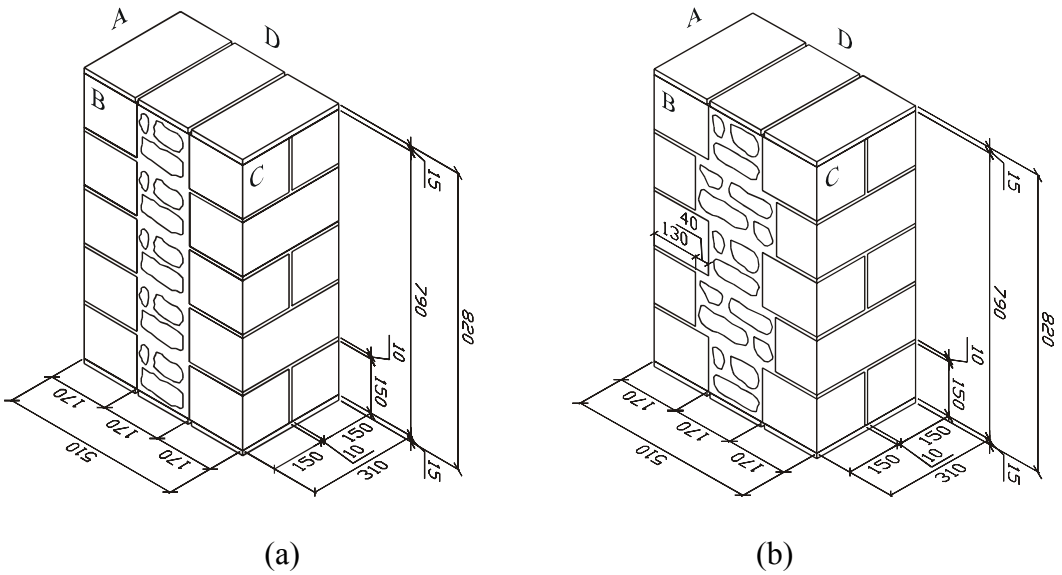

(a) (b)

Figure 1. Wallets dimensions in *mm*: (a) straight collar joints and (b) keyed collar joints.

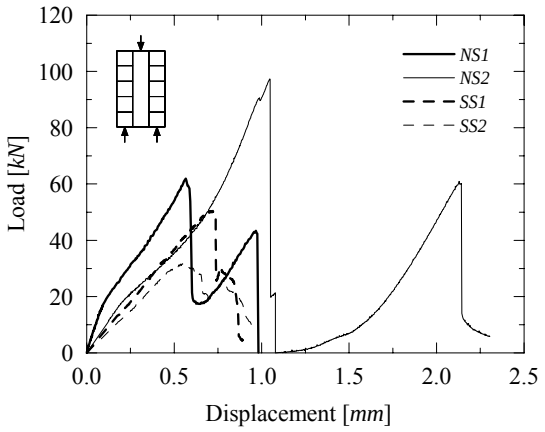

(a)

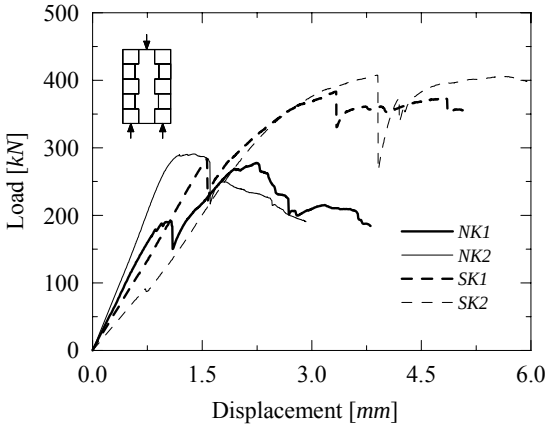

(b)

Figure 2. Load-displacement diagrams obtained for the shear tests using the testing machine in-built displacement transducer: (a) straight collar joints and (b) keyed collar joints.

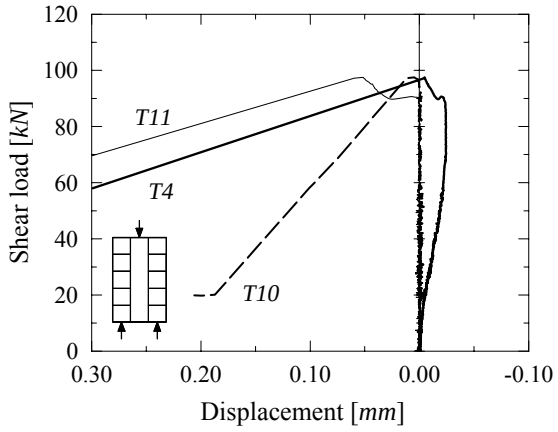

(a)

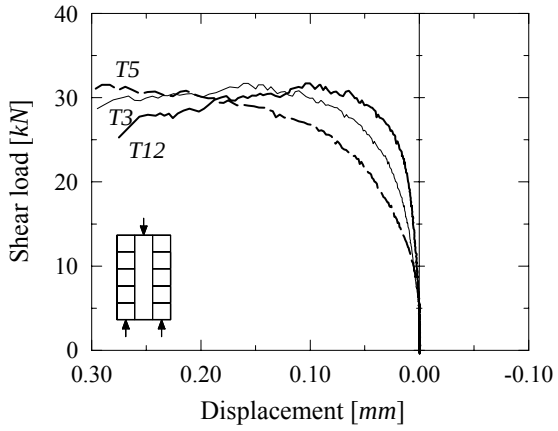

(b)

Figure 3. Load-displacement diagrams obtained for wallets with straight collar joints using displacement transducers fixed to the specimens faces: (a) *Noto* specimen (*NS2*) and (b) *Serena* specimen (*SS2*). Positive sign is adopted for elongation and negative for contraction.

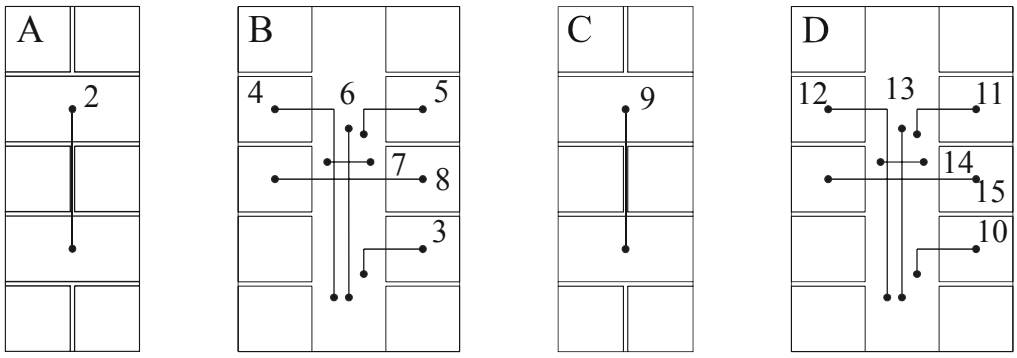

Figure 4. Position of the transducers for wallets *NS2* and *SS2*.

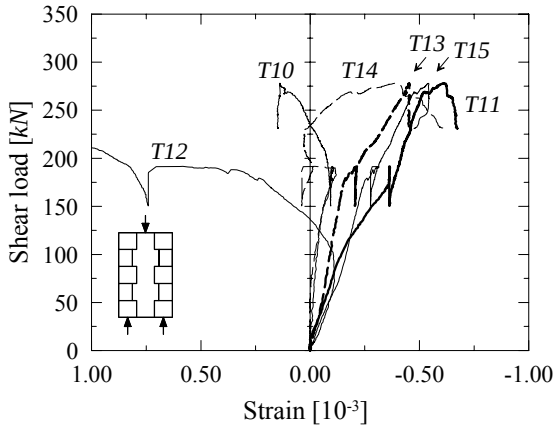

(a)

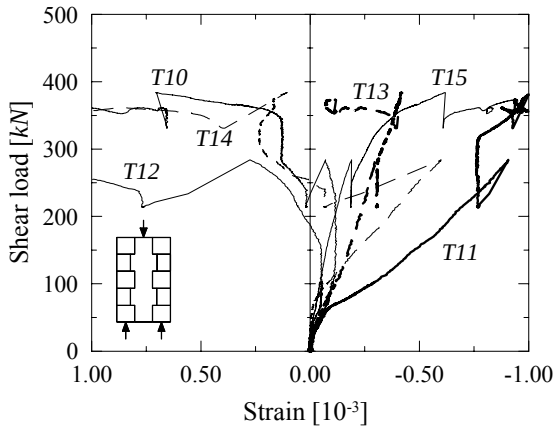

(b)

Figure 5. Load-displacement diagrams obtained for wallets with keyed collar joints using displacement transducers fixed to the specimens faces: (a) *Noto* specimen (*NK1*) and (b) *Serena* specimen (*SK1*). Positive sign is adopted for elongation and negative for contraction.

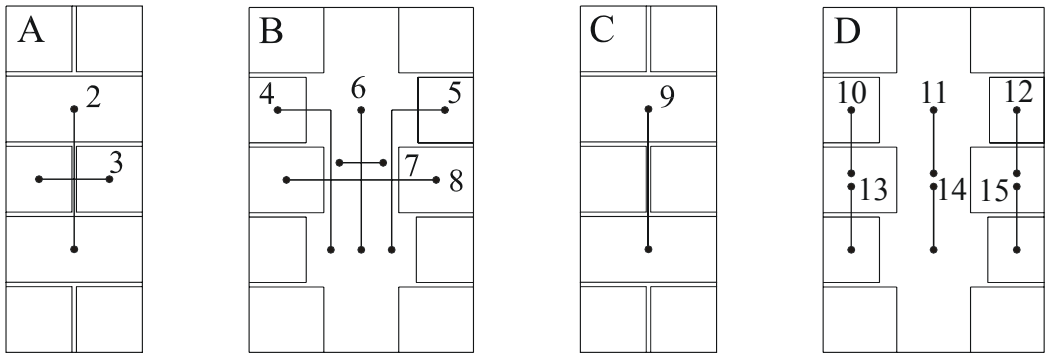

Figure 6. Position of the transducers for wallets *NK1* and *SK1*.

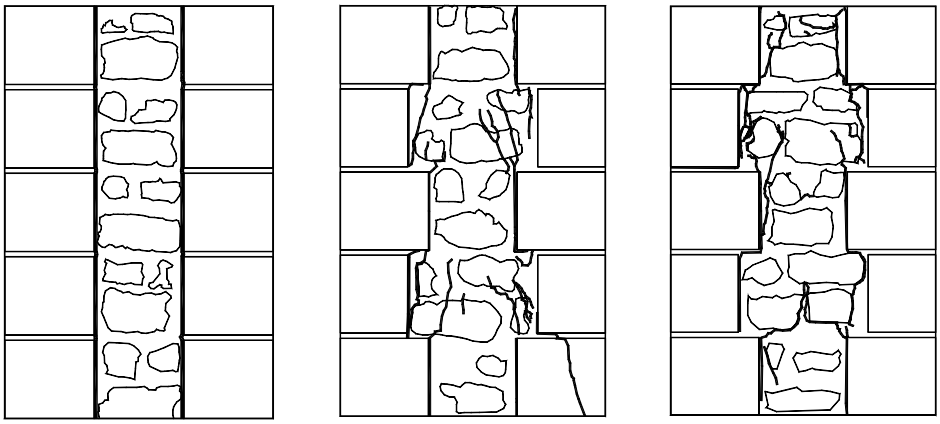

(a) (b) (c)

Figure 7. Typical ultimate crack patterns for (a) straight collar joints wallets (*NS1*) and keyed collar joints wallets: (b) *Noto* (*NK1*) and (c) *Serena* (*SK2*).

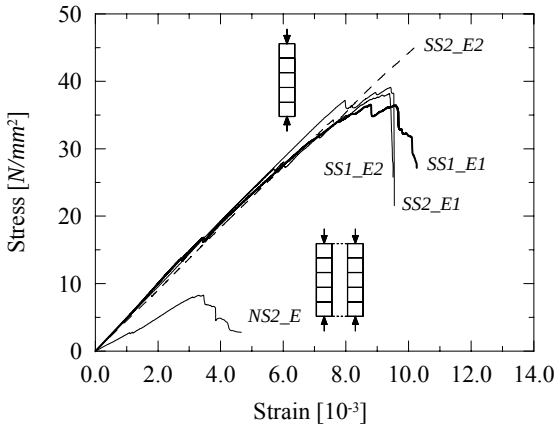

(a)

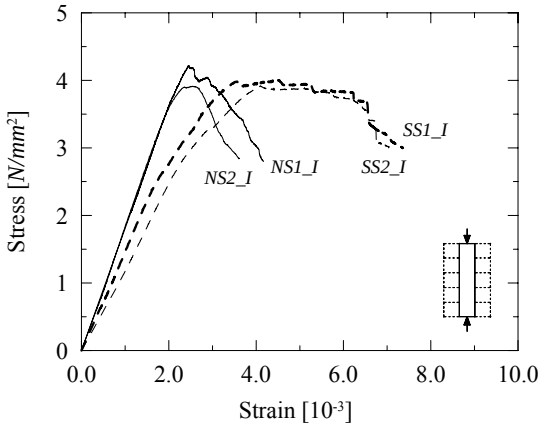

(b)

Figure 8. Stress-strain diagrams obtained from compression tests on single leaves using the testing machine in-built displacement transducer: (a) outer-leaves and (b) inner-leaves. A problem in the acquisition system prevented fully capturing the *NS1_E* diagram and, thus, it is not shown. It is also noted that failure of specimen *SS2_E2* could not be attained within the capacity of the testing machine.

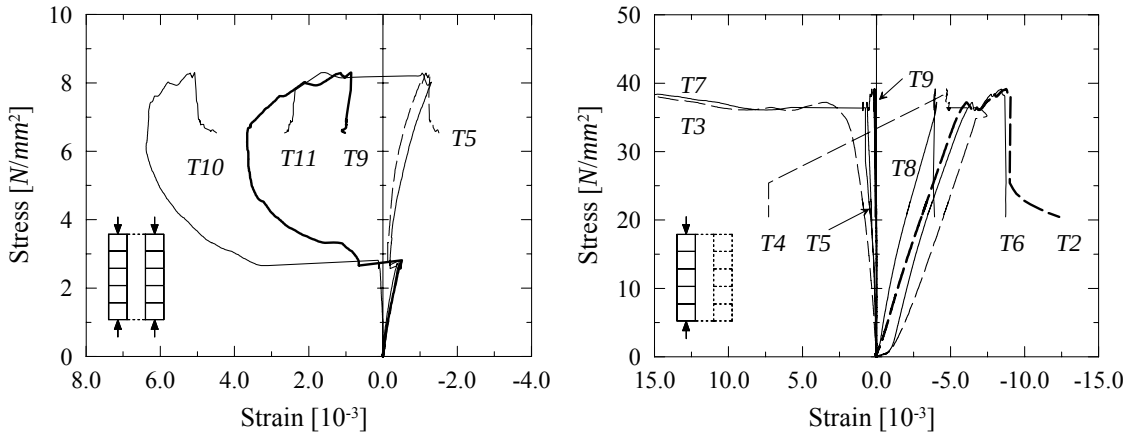

Figure 9. Stress-strain diagrams obtained from compression tests on outer-leaves using the displacement transducers attached to the specimens: (a) *NS2_E* and (b) *SS2_E1*. Positive sign is adopted for elongation and negative for contraction.

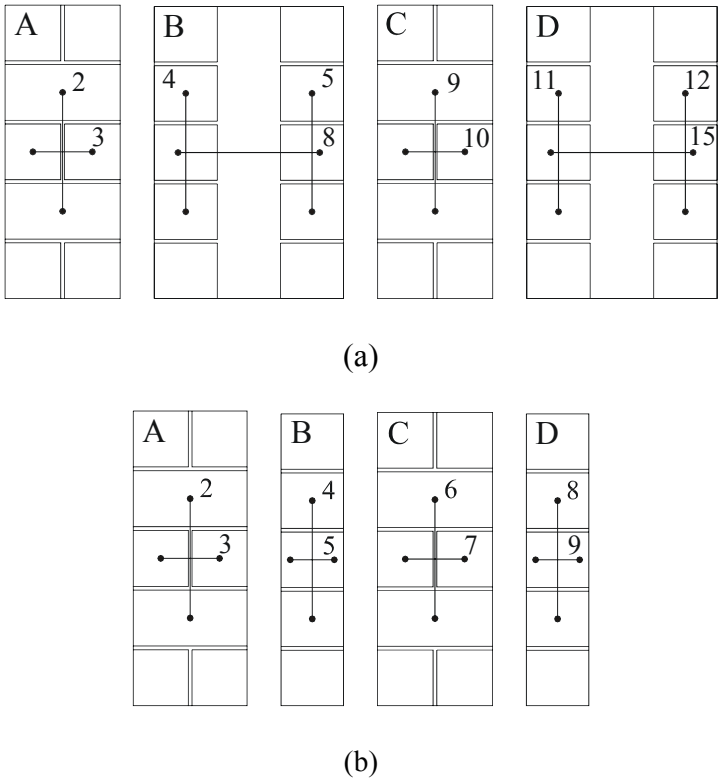

Figure 10. Position of the transducers for (a) *NS2_E* and (b) *SS2_E1*.

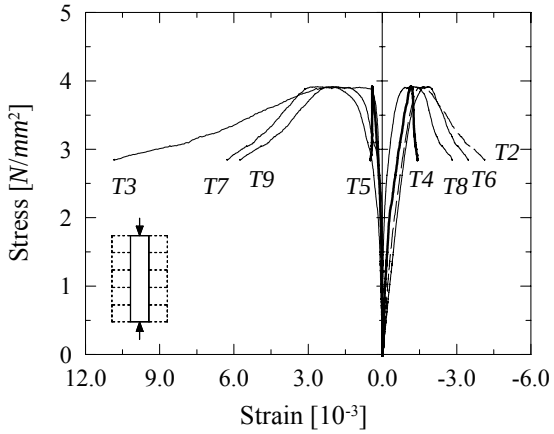

(a)

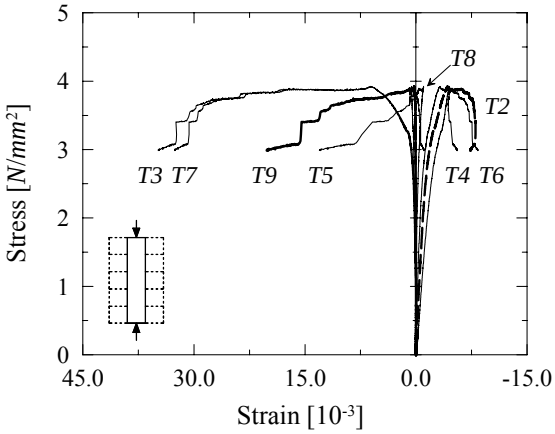

(b)

Figure 11. Stress-strain diagrams obtained from compression tests on inner-leaves using the displacement transducers attached to the specimens: (a) *NS2_I* and (b) *SS2_I*. Positive sign is adopted for elongation and negative for contraction.

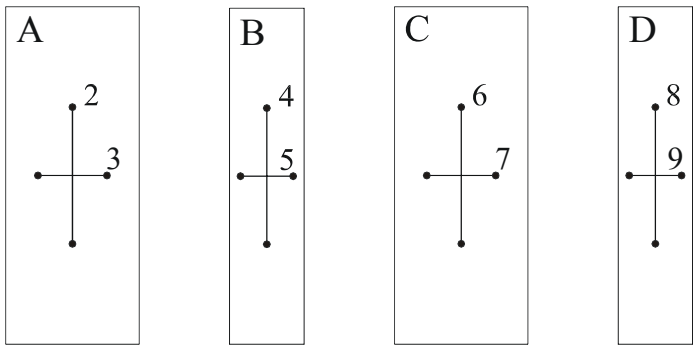

Figure 12. Position of the transducers for (a) *NS2_I* and (b) *SS2_I*.

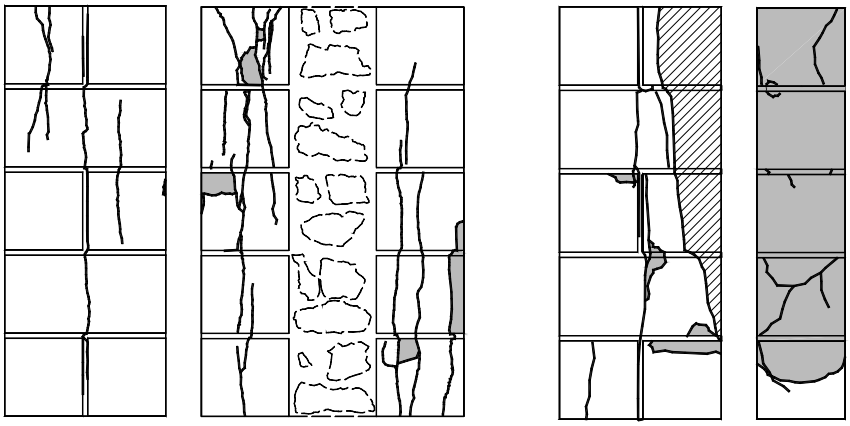

(a) (b)

Figure 13. Typical ultimate failure patterns for the outer-leaves: (a) *Noto* stone and (b) *Serena* stone.

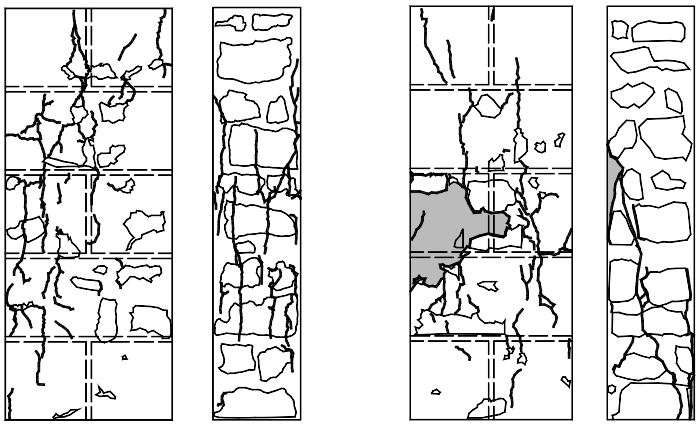

(a) (b)

Figure 14. Typical ultimate failure patterns for the inner-leaves: (a) *Noto* stone and (b) *Serena* stone.

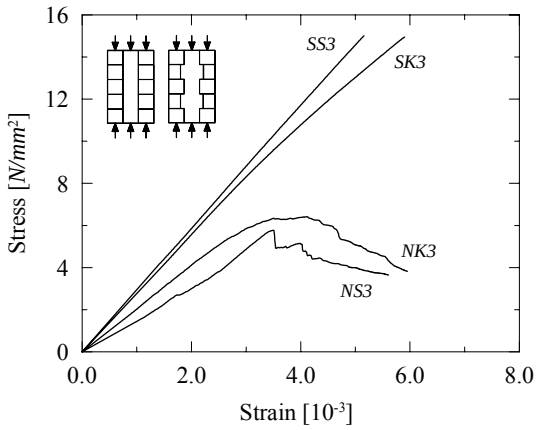

Figure 15. Stress-strain diagrams obtained from compression tests on full wallets using the testing machine in-built displacement transducer.

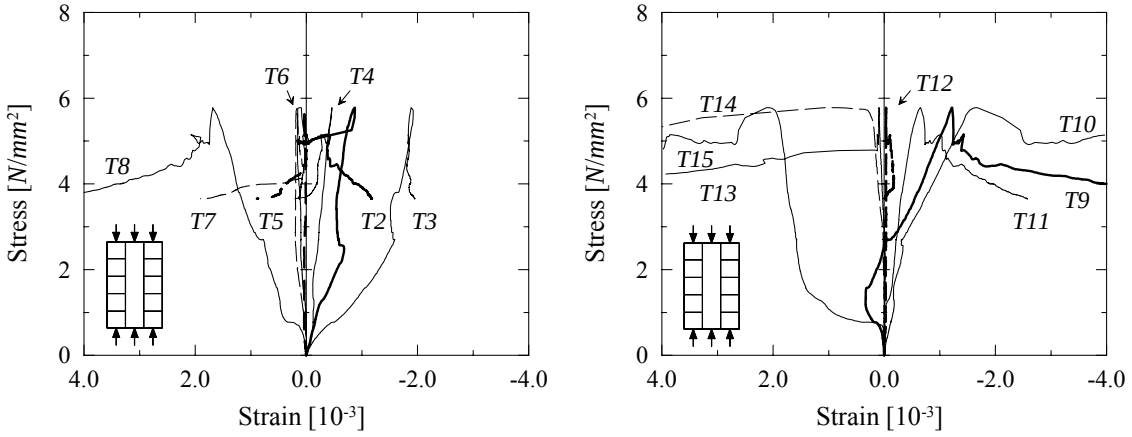

(a)

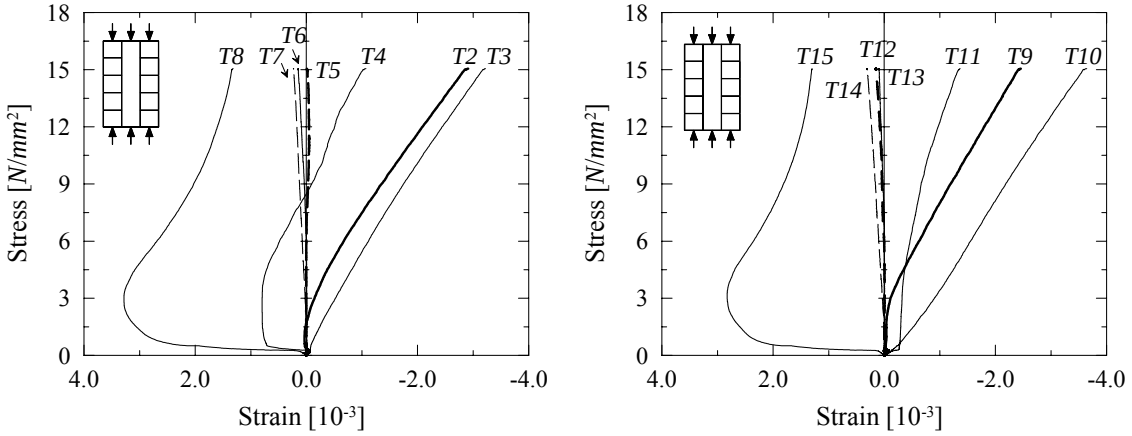

(b)

Figure 16. Stress-strain diagrams obtained for wallets with straight collar joints using displacement transducers fixed to the specimens faces: (a) *Noto* (*NS3*) and (b) *Serena* (*SS3*). Positive sign is adopted for elongation and negative for contraction.

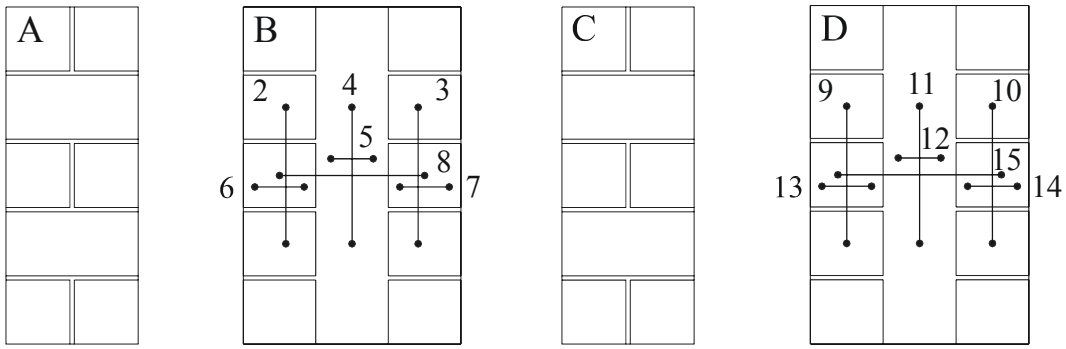

Figure17. Position of the transducers for wallets *NS3* and *SS3*.

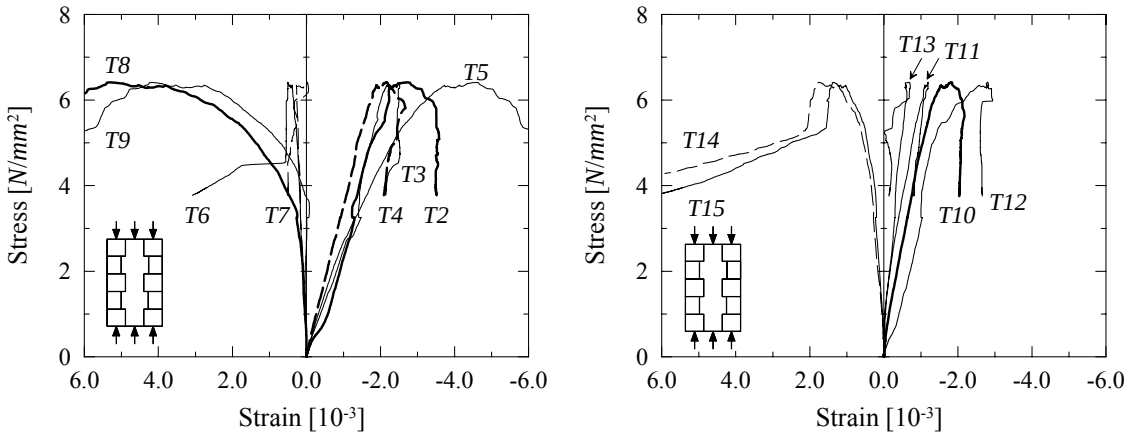

(a)

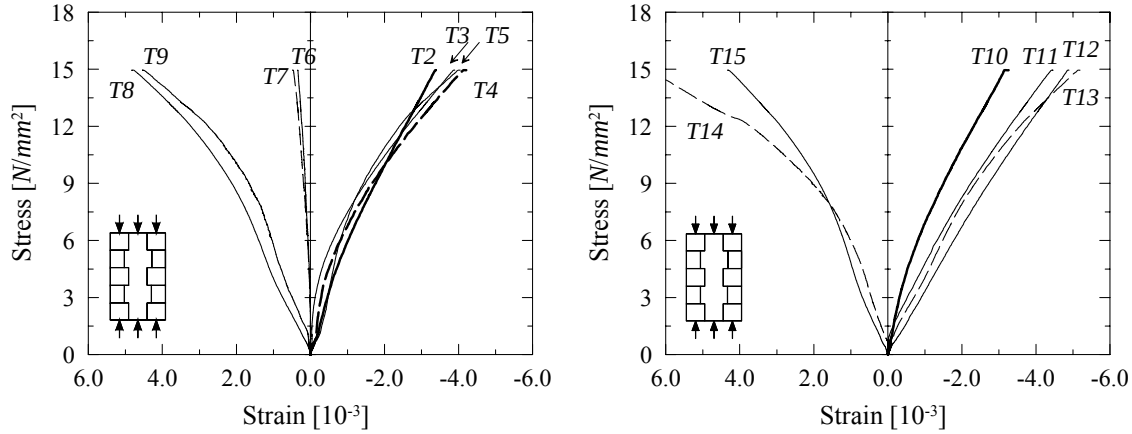

(b)

Figure 18. Stress-strain diagrams obtained for wallets with keyed collar joints using displacement transducers fixed to the specimens faces: (a) *Noto* (*NK3*) and (b) *Serena* (*SK3*). Positive sign is adopted for elongation and negative for contraction.

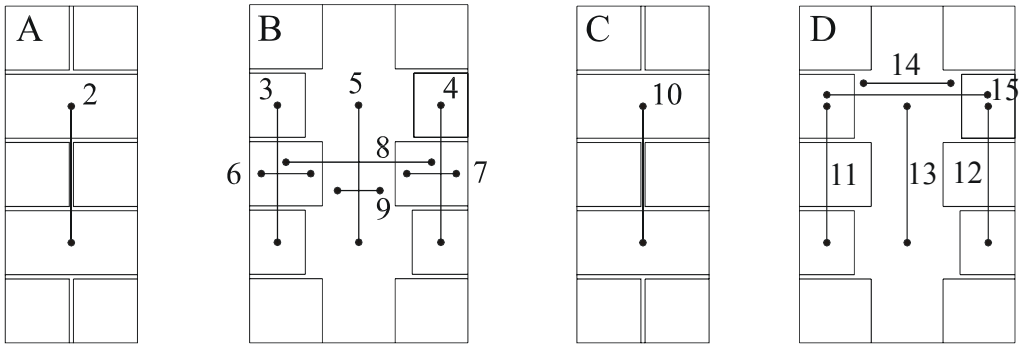

Figure 19. Position of the transducers for wallets *NK3* and *SK3*.

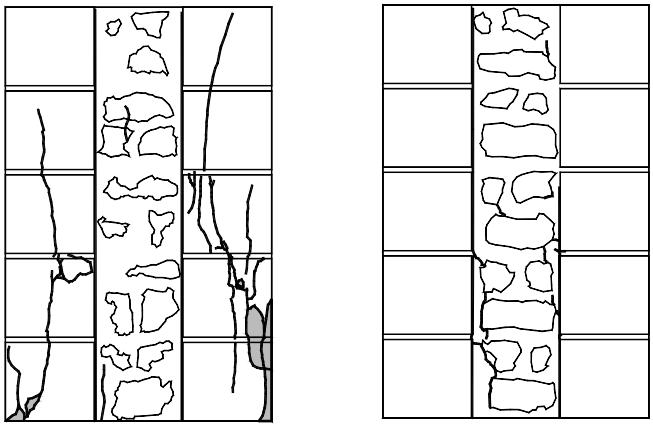

(a) (b)

Figure 20. Ultimate failure patterns for the wallets with straight collar joints: (a) *Noto* (*NS3*) and (b) *Serena* (*SS3*).

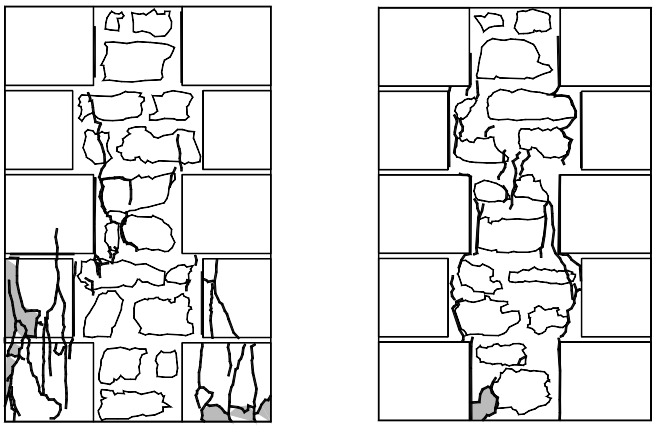

(a) (b)

Figure 21. Ultimate failure patterns for the wallets with keyed collar joints: (a) *Noto* (*NK3*) and (b) *Serena* (*SK3*).

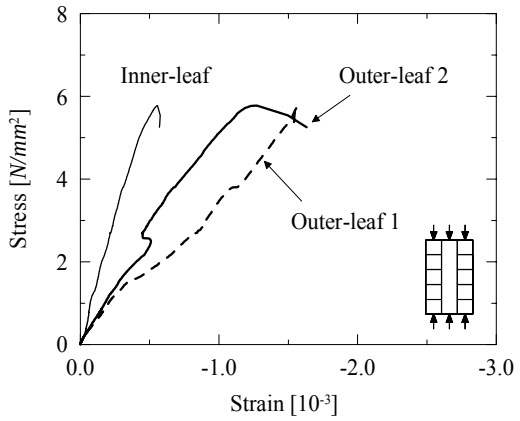

(a)

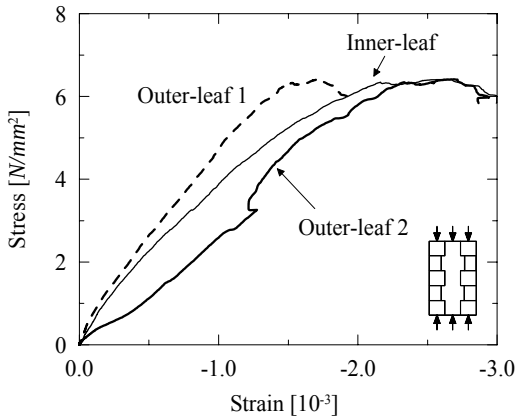

(b)

Figure 22. Compression stress-strain diagrams of the leaves inside the *Noto* wallets: (a) straight collar joints (*NS3*) and (b) keyed collar joints (*NK3*). It is noted that the stress values represent average values obtained from the external load. Moreover, deformation values were obtained from the transducers shown in Figure 17 for straight collar joints wallets (outer-leaf 1: *T2* and *T10*; outer-leaf 2: *T3* and *T9*; inner-leaf: *T4* and *T11*) and in Figure 19 for keyed collar joints wallets (outer-leaf 1: *T2*, *T3* and *T12*; outer-leaf 2: *T4*, *T10* and *T11*; inner-leaf: *T5* and *T13*).

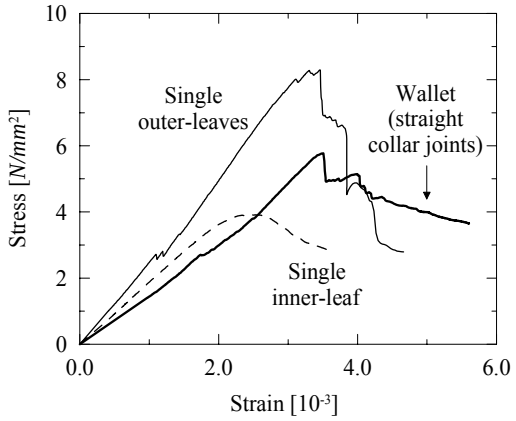

(a)

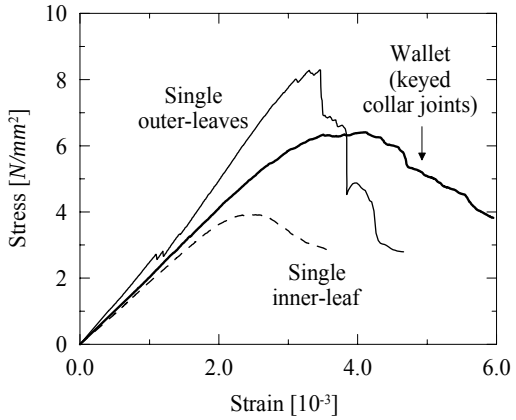

(b)

Figure 23. Comparison between the compression stress-strain diagrams obtained from the single inner and outer-leaves and from the full wallets, built with the *Noto* stone: (a) straight collar joints (*NS3*) and (b) keyed collar joints (*NK3*). Deformations were measured using the testing machine in-built displacement transducer.

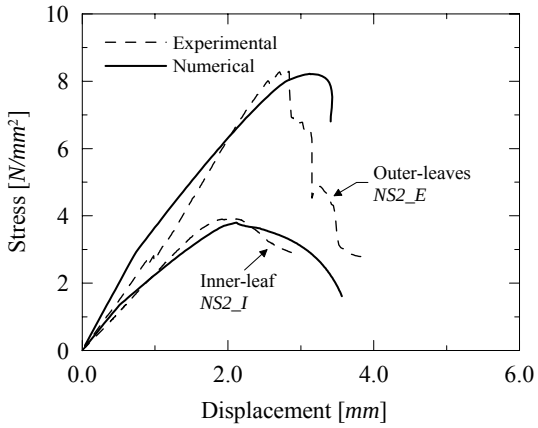

Figure 24. Compression stress-displacement diagrams for the leaves of the *Noto* wallets.

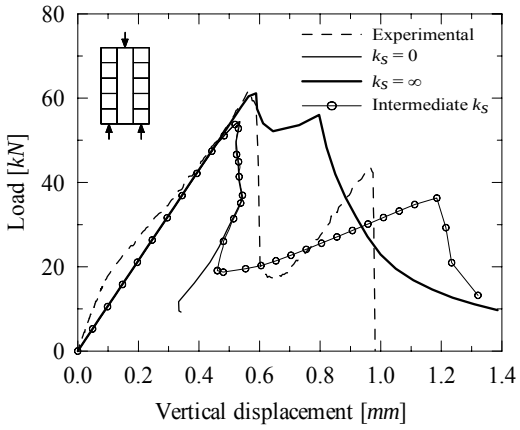

(a)

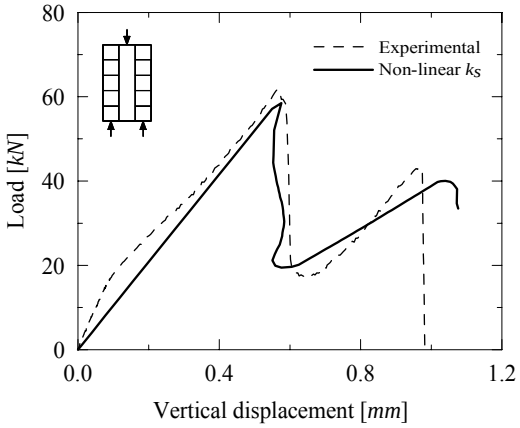

(b)

Figure 25. Numerical and experimental (*NS1*) shear load-displacement diagrams for straight collar joints wallets. Different shear stiffnesses were considered at boundaries: (a) constant and (b) non-linear.

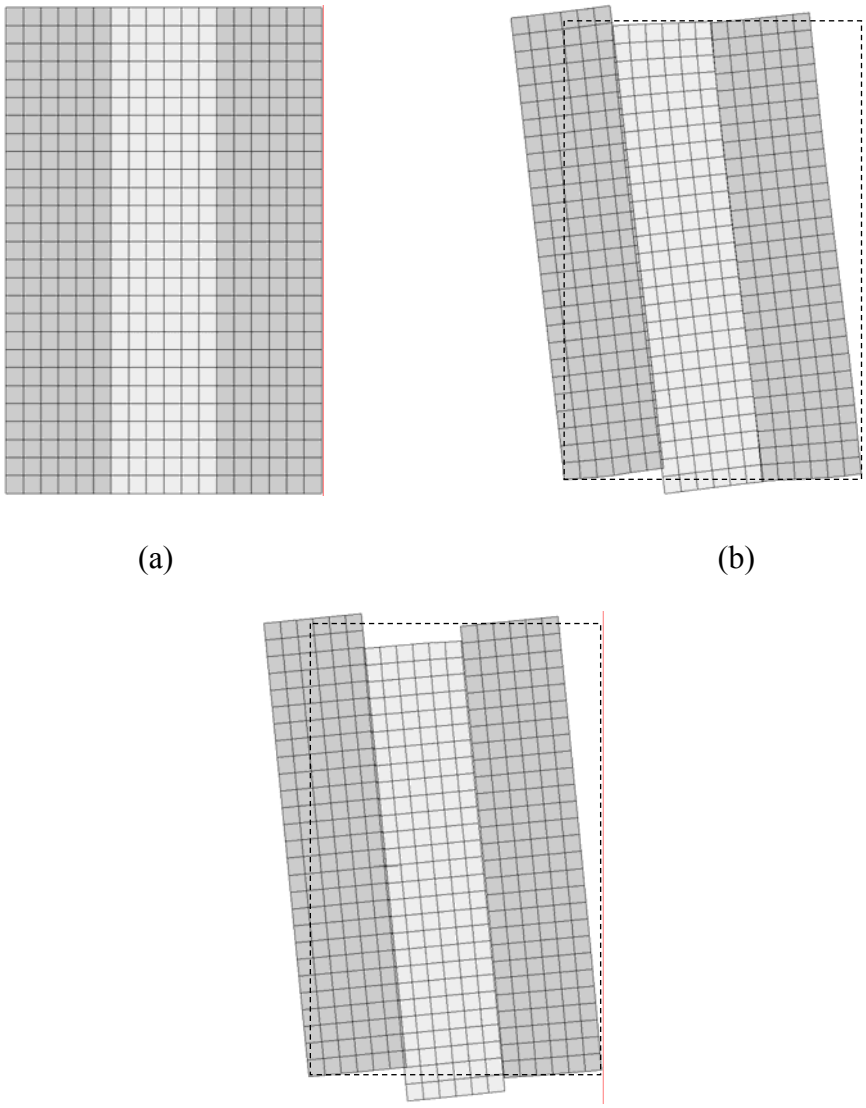

Figure 26. Progressive shear failure for non-linear k_s boundary conditions: (a) mesh adopted, (b) deformed (incremental) mesh after failure of the first connection and (c) deformed (total) mesh after failure of the second connection.

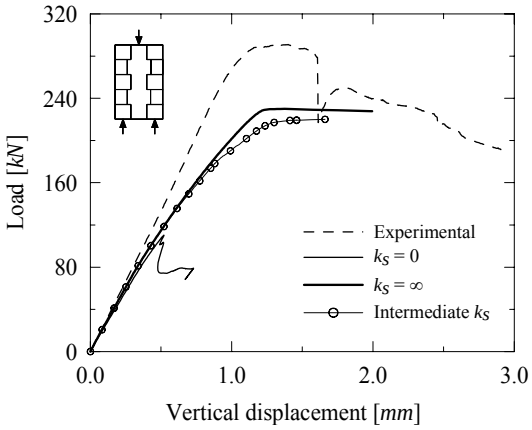

Figure 27. Numerical and experimental (*NK2*) shear load-displacement diagrams for keyed collar joints wallets. Different shear stiffnesses k_s were considered at the boundaries.

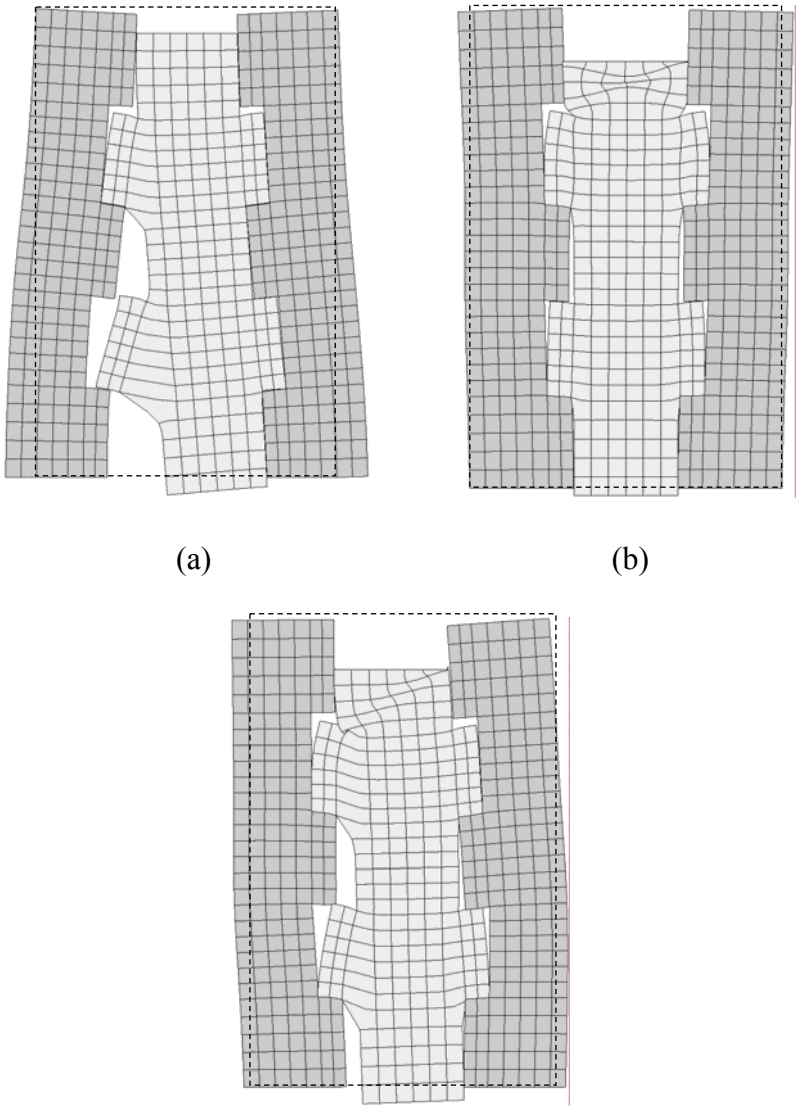

Figure 28. Deformed meshes at failure for different shear stiffnesses k_s at the supports: (a) $k_s = 0$, (b) $k_s = \infty$ and (c) intermediate k_s.

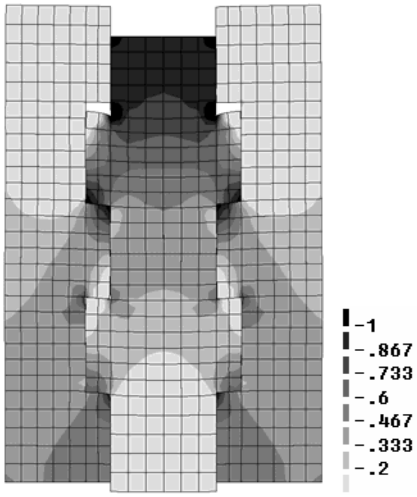

(a)

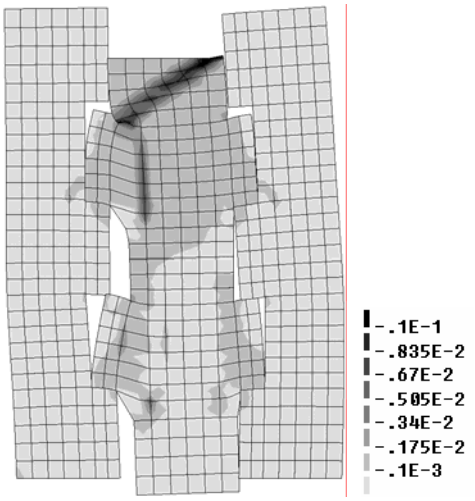

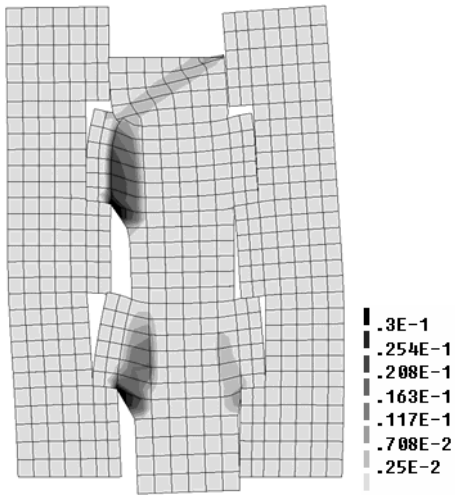

(b) (c)

Figure 29. Results obtained for the shear simulations on keyed wallets, adopting the intermediate k_s: (a) principal minimum stresses for an applied load of 50 *kN* (elastic regime) and principal plastic strains at failure: (b) minimum and (c) maximum.

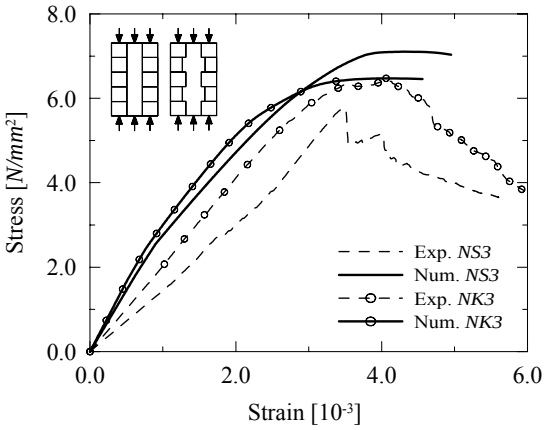

Figure 30. Compression stress-strain diagrams obtained on wallets with straight collar joints (*NS3*) and keyed collar joints (*NK3*).

TABLES

Table 1. Designation of the tested wallets. The first letter corresponds to the type of stone (*N* for *Noto* and *S* for *Serena*) while the second letter stands for the type of connection (*S* for straight and *K* for keyed).

	Straight collar joints	Keyed collar joints
Noto limestone	*NS1*, *NS2*, *NS3*	*NK1*, *NK2*, *NK3*
Serena sandstone	*SS1*, *SS2*, *SS3*	*SK1*, *SK2*, *SK3*

Table 2. Average results for the bulk density and open porosity of the stones.

Type of stone	$\rho_{b,s}$ kg/m^3	CV %	P_o %	CV %
Noto	1760	1.5	15.4	4.5
Serena	2570	0.3	2.1	5.7

Table 3. Average results obtained from the compression tests on the stones (values in brackets give the *CV*).

Type of stone	Orientation	f_c N/mm^2	ε_p 10^{-3}	E N/mm^2	ν -
Noto	*L*	20.6 (7%)	2.4	9475	0.10
Noto	*B*	17.6 (22%)	2.3	8525	0.09
Serena	*L*	104.2 (1%)	[a]	18218	0.19
Serena	*B*	89.0 (15%)	[a]	23293	0.21

[a] The *Serena* specimens had to be tested in a machine with a higher capacity, which did not allow recording the displacement values.

Table 4. Average results obtained from the tension tests on the stones

(values in brackets give the *CV*).

Type of stone	Orientation	$f_{t,s}$ N/mm^2	f_t N/mm^2
Noto	*B*	2.05 (13%)	1.8
Serena	*B*	6.00 (12%)	5.4

Table 5. Average results obtained from the flexural and compression tests on the mortar (values in brackets give the *CV*).

Curing time *Days*	f_f N/mm^2	f_c N/mm^2
28	1.5 (6%)	7.4 (3%)
75	1.9 (13%)	9.2 (6%)
90	2.3 (10%)	9.7 (7%)
172	2.2 (9%)	11.2 (5%)

Table 6. Average results obtained from the shear tests.

Wallets	Type of stone	Type of connection	τ_r N/mm^2	δ mm	τ_r' N/mm^2	δ' mm
NS1, *NS2*	*Noto*	Straight	0.17	0.81	0.22	1.55
SS1, *SS2*	*Serena*	Straight	0.09	0.64	0.11	0.78
NK1, *NK2*	*Noto*	Keyed	0.58	1.82	-	-
SK1, *SK2*	*Serena*	Keyed	0.81	3.62	-	-

Table 7. Average results obtained from the compression tests on single leaves.

Specimen	Type of stone	Type of leaf	Peak load *kN*	f_c N/mm^2	ε_p 10^{-3}	E N/mm^2	ν -
NS_E	*Noto*	outer	912	8.7	3.3	3150	-
SS_E	*Serena*	outer	2095	39.8	9.5	4870	-
NS_I	*Noto*	inner	214	4.1	2.6	1830	0.15
SS_I	*Serena*	inner	209	4.0	4.3	1405	0.18

Table 8. Results obtained from the compression tests on full wallets.

Wallet	Type of stone	Type of connection	Peak load *kN*	f_c N/mm^2	ε_p 10^{-3}	E N/mm^2
NS3	*Noto*	straight	913	5.8	3.5	1770
SS3	*Serena*	straight	> 2380	> 15.1	> 5.2	2940
NK3	*Noto*	keyed	1013	6.4	4.1	2085
SK3	*Serena*	keyed	> 2380	> 15.1	> 5.9	2725

Table 9. Predicted compressive strength values for the tested wallets.

Wallet	Type of stone	Type of connection	Experimental f_c N/mm^2	Predicted f_c $[N/mm^2]$		
				Eq. (1)	Eq. (2)	Eq. (3)
NS3	*Noto*	straight	5.8	5.8	7.2	5.8
SS3	*Serena*	straight	> 15.1	25.3	26.6	19.4
NK3	*Noto*	keyed	6.4	-	6.4	5.7
SK3	*Serena*	keyed	> 15.1	-	21.3	16.1

Table 10. Elastic properties for the wallets leaves.

Material	E N/mm^2	ν -
Outer-leaves	3150	0.10
Inner-leaf	2100	0.15

Table 11. Inelastic properties for the wallets leaves.

Material	c N/mm^2	f_t N/mm^2	$\sin \phi$ -	$\sin \psi$ -	Gf_c[(a)] N/mm	Gf_I[(b)] N/mm
Outer-leaves	3.7	1.8	0.17	0.09	5.0	0.070
Inner-leaf	1.7	0.3	0.17	0.09	5.0	0.035

[(a)] The values given for the compressive fracture energy are cohesion related.

[(b)] For the shear simulations of the keyed wallets, the values adopted for Gf_I were 0.150 (outer-leaves) and 0.070 *N/mm* (inner-leaf), so that numerical convergence could be achieved.

Table 12. Elastic properties for the collar joints.

Collar joint	k_n N/mm^3	k_s N/mm^3
1 (left)	150	0.4
2 (right)	150	0.4

Table 13. Inelastic properties for the collar joints.

Collar joint	c N/mm^2	f_t N/mm^2	$\tan \phi$ -	$\tan \psi$ -	Gf_I N/mm	Gf_{II} N/mm
1 (left)	0.13	0.09	0.70	0.00	0.015	0.050
2 (right)	0.21	0.14	0.70	0.00	0.015	0.060